Self-Powered Cardiac Monitoring: Maintaining Vigilance with Multi-Modal Harvesting and E-Textiles

Luis Lopez Ruiz, Student Member, IEEE, Matthew Ridder, Dawei Fan, Jiaqi Gong, Member, IEEE, Braden Max Li, Amanda Myers, Elizabeth Cobarrubias, Jason Strohmaier, Jesse Jur and John Lach, Senior Member, IEEE

***Abstract*— Remote patient monitoring has emerged from the intersection of engineering and medicine. Advances in sensors, circuits and systems have made possible the implementation of small, wearable devices capable of collecting and streaming data for long periods of time to help physicians track diseases and detect conditions in a non-intrusive manner. Cardiac monitoring comprises many of these applications, with the need to capture transient cardiac events motivating the adoption of wearable monitors in standard clinical practice. However, user burden and battery life limit the duration of monitoring or require heavy duty cycling, thus preventing the adoption of these technologies for use cases that require long-term vigilant monitoring, in which the sensor system cannot miss a critical cardiac event. To overcome these challenges, this paper introduces a self-powered system for uninterrupted vigilant cardiac and activity monitoring that senses and streams electrocardiogram (ECG) and motion data continuously to a smartphone while consuming only 683 µW on average. To achieve self-powered operation under environmental and wearability constraints, the system incorporates an energy combining technique to support multi-modal energy harvesting from indoor solar and thermoelectric energy. A custom ECG shirt made of a knitted compression fabric with embedded dry electrodes addresses issues of user comfort, skin irritation and motion artifacts. Vigilant Atrial Fibrillation (AF) monitoring is used as an example case study, analyzing sampling frequency and bit-depth quantization and their correlation to vigilant, self-powered operation. The integrated system demonstrates an important step forward for remote patient monitoring beyond the clinic.**

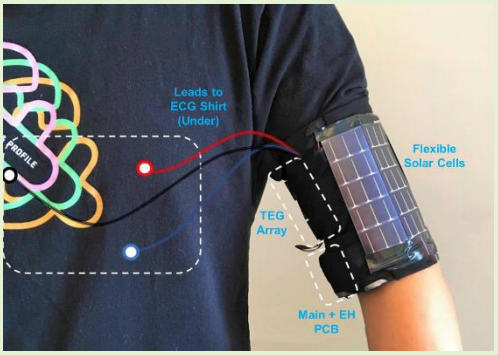

***Index Terms*— atrial fibrillation, Bluetooth, body sensor networks, cyber-physical systems, energy harvesting, e-textiles, low-power electronics, remote monitoring, self-powered, smart textiles, wearable, wireless**

1

I. Introduction

IN a 2018 study, the American Heart Association reported Cardiovascular Disease (CVD) as a leading cause of death in the United States and an associated cost of $555 billion driven by the elevated number of hospitalizations and re-hospitalizations of patients with CVD due to the aggravation of symptoms [1, 2]. In response to this, researchers and physicians have looked at remote patient monitoring as a potential solution to provide affordable and effective care by eliminating unnecessary visits, improving communication and treatment, and optimizing the allocation of resources in the clinic [3]. Furthermore, specific recommendations have emphasized the integration of telehealth and mobile health technologies as part of this effort [1]. A variety of home health technologies have seen some success, but the associated user burden often results in infrequent samples of physiological status. Cyber-physical sensor systems such as body sensor networks (BSNs) can alleviate many of the issues found in current remote patient monitoring methods by collecting, processing and transmitting high quality physiological, activity, and environmental data. However, critical obstacles need to be overcome before these technologies can be comprehensively adopted [4].

User compliance and battery life represent two such obstacles. The implications of these issues are commonly reflected in the willingness of the user to wear the device, the system losing power during the deployment, or the effects of the latter on the former by having the user frequently recharge the device. To address user acceptance, researchers have made

Research supported by the U.S. National Science Foundation under grants number EEC-1160483 and CNS-1646454.

Luis Lopez Ruiz is with Charles L. Brown Department of Electrical and Computer Engineering, UVA Link Lab, University of Virginia, Charlottesville, VA 22904 USA (e-mail: ljl2wf@virginia.edu).

Dawei Fan and Matthew Ridder were with Charles L. Brown Department of Electrical and Computer Engineering and Department of Computer Science, UVA Link Lab, University of Virginia, Charlottesville, VA 22904 USA (e-mail: {df5ah ,mjr3vk}@virginia.edu).

Jiaqi Gong is with Department of Information Systems, University of Maryland, Baltimore County, Baltimore, MD 21250 USA (email: jgong@umbc.edu).

Braden Max Li, Amanda Myers, Elizabeth Cobarrubias and Jesse Jur are with the Wilson College of Textiles, North Carolina State University, Raleigh, NC 27606 USA (e-mail: {bmli, acmyers3, ecobarr, jsjur}@ncsu.edu).

Jason Strohmaier was with Department of Electrical and Computer Engineering, North Carolina State University, Raleigh, NC 27606 USA (e-mail: jmstrohm@ncsu.edu).

John Lach is with Department of Electrical and Computer Engineering, The George Washington University, Washington, DC 20052 USA (e-mail: jlach@gwu.edu).

This paper is an extension of the work presented at BioCAS 2017 and BSN 2018 (https://ieeexplore.ieee.org/document/8325126, https://ieeexplore.ieee.org/document/8329695).

innovations related to form factor, operation and maintenance [5]. In addition, multiple efforts have been made to develop ultra-low power electronics to increase battery life or even to replace the battery itself by harvesting energy from the environment or the body [6]. However, achieving these operating conditions typically requires reduced sampling rates and duty cycling, which may result in missed critical cardiac and activity events, relegating the system incapable of providing vigilant monitoring.

Achieving long-term vigilance in a self-powered system requires continuously maintaining a positive energy balance. Energy harvesters have been developed for BSNs to scavenge solar energy from the environment, and heat and motion from the body, but form factors, low conversion efficiencies, and variable energy availability have proven to be difficult challenges. Several approaches to efficiently administer the harvested energy have been presented from a hardware and software perspective. In the case of the former, the individual blocks of the energy harvesting and power management unit (PMU) have been optimized for self-powered applications [7]. In the latter, dynamic power management (DPM) techniques have been developed to adjust the operation of the system based on workload, available energy, and required data quality [8, 9]. Even though previous works have investigated the relationship of data quality and power consumption, many of these approaches consider digital signal metrics that may or may not relate to application-level information metrics, such as critical event detection vigilance.

This paper addresses these issues by expanding the work reported in [10, 11] and using an application-driven approach to define the system design space that drives the design of a self-powered wearable sensor system with e-textile integration for vigilant cardiac and activity monitoring that achieves a positive energy balance solely from solar and thermal energy but also has the flexibility to be interfaced with other harvesting modalities. The system includes wireless streaming to a smartphone programmed both to process and display the data, and to interface with web services and applications for remote data access and caregiver/clinician notification. Specific contributions of this work include:

a. A multi-modal energy harvesting architecture that combines the harnessed energy from solar cells and thermoelectrical generators (TEGs) to power the wearable sensor system, and which stores the surplus of energy into a supercapacitor for when not enough energy at the input is available.
b. A custom compression electrocardiogram (ECG) shirt with embedded dry-electrodes to improve wearability, user compliance, and reduce motion artifacts.
c. A formalization of *vigilance* in the context of wearable sensing systems as an additional dimension to a previously proposed taxonomy for health applications.
d. A demonstration of vigilant monitoring for atrial fibrillation (AF) as a case study through the assessment of sampling frequency and bit-depth quantization and their relationship with system power consumption to achieve self-powered operation.

The remainder of the paper is organized as follows. Section II discusses background and related work, including a discussion of self-powered systems and a definition of "vigilance" in the context of sensor systems. Section III presents the end-to-end wearable sensor system, followed by the description of the textile integration and the modeling of the system power consumption in Section IV and Section V, respectively. AF as a case study and as a driver of the design space and metrics for the system is analyzed in Section VI, and a comparison with state-of-the-art wearable cardiac monitors is summarized in Section VII. Deployment results and considerations for preserving both vigilance and a positive energy balance are presented within the context of that use case in Section VIII. Finally, conclusions and future work are discussed in Section IX.

II. Background And Related Work

Developing a framework for self-powered sensor systems for vigilant cardiac monitoring requires the integration of multiple elements that need to be designed and optimized to work together in a harmonious way. Therefore, we review previous advances in wearables for health applications, self-powered sensor systems, and cardiac and activity monitoring systems, while also clarifying the meaning of "vigilance" in this context.

A. Wearable Systems for Health Applications

The miniaturization of technology has enabled the development of sensor systems that can be attached to the body with purposes that range from disease diagnosis and tracking to physical rehabilitation and behavior modification. For instance, in [6] the authors discuss the design of a system intended for improving the understanding of the impact of increased ozone levels and other pollutants on chronic asthma conditions. Similarly, the authors Han et al. reported in [12] a piezoelectric based system embedded in a shoe sole to identify different forms of human motion. Furthermore, a system designed for motion monitoring during physical rehabilitation is presented in [13]. Given this wide range of efforts in wearables for health applications, Witte et al. conducted a systematic literature review of state-of-the-art devices reported from 2013 to 2018 [14]. The authors conducted an extensive search on four different research literature databases, selecting 200 papers from each database as a representative sample based on relevance for their fields. After multiple filters using a predefined criterion, 97 papers were selected for the systematic review. To analyze the reported works, the authors classified the papers based on disease treatment, application area, vital parameter measurement and target patients. From this evaluation, five potential research areas were identified: application scenarios for widespread diseases, expansion of wearable systems functionality, diversity of vital parameters measurement, proactive analysis of sensor data for preventive purposes and promoting patient adoption through enhanced usability.

A comparable exercise done by Pevnick et al. in [15] for cardiac monitoring proposed a taxonomy to classify wearable sensor systems in the general context of health applications based on the data collection mechanism. Such classification

was established according to the patient engagement required (passive vs. active), the data acquisition mode (continuous vs. intermittent) and the data management mode (streaming vs. storing). As a result, each reported wearable device could be categorized based on the patient engagement and the data acquisition and management modes employed. However, a limitation of this categorization is the broad definition of continuous collection, which does not differentiate between continuous monitoring and vigilant monitoring.

A different approach taken by researchers has been the development of application specific integrated circuits (ASIC) with subsystems designed, optimized, and highly integrated on a single chip or package for wearable and health applications. For instance, a system-on-chip (SoC) presented in [16] proposes an event-driven architecture that allows for clockless operation and power reduction. The SoC has an ultra-wideband transmitter for wireless communication and it consumes 2.89 μW when operating at 1.2V. A comparable effort was proposed in [17] where an ASIC front-end for biosensing was optimized for noise, power, and area. These optimizations give the chip the flexibility of sensing different biopotentials by adjusting parameters such as gain and filter cutoff frequency. The chip consumes 5.74 μW plus 306 nW for the power management unit and it is all packed in an area of 0.0228 mm^2. Another example of this approach is the work introduced in [18] where a highly integrated SoC incorporates subsystems for sensing, processing and control, wireless communication, energy harvesting and power management, and application-specific accelerators for wearable sensors. The SoC is able to operate from different harvesters with high efficiency without the need of additional energy sources and employs an ultra-wide band transmitter for wireless communication. The full system consumes 6.45 μW in a motion capture application, powered from indoor solar by the energy harvesting and power management unit.

B. Vigilant Monitoring

In the context of sensor systems, the term “vigilant” has a specific meaning – a vigilant monitoring system is one that operates in a mode such that no critical events are missed. Events may be missed due to noise or user error, but not due to operational mode. It is important to note the difference between *vigilant* sensing and *continuous* sensing, as a continuous sensing system may not include all of the necessary sensors or operate at the minimum sampling frequency and/or quantization bit depth to ensure that all critical events will be detected. Conversely, not all vigilant systems perform continuous sensing, as critical events may only happen during certain times, activities, etc., and the system does not need to operate otherwise. To design a monitoring system to be vigilant, a precise definition of a critical event must be established and is inherently application dependent. For the use case application explored in this paper, a critical event is AF (which can be short in duration and can happen intermittently and irregularly) as detected through ECG monitoring using a state-of-the-art AF classification algorithm.

C. Energy Harvesting

Harvesting energy from the environment represents a promising option to overcome the limitations of battery-powered wireless sensor nodes. Multiple efforts have been made to advance various energy harvesting modalities, leading to the realization of self-powered sensor systems. In a survey presented by Panatik et al. [19], the authors researched the work done in harvesting mechanical, solar, thermal and fluid flow energy. A similar study was done in [20], where Singh and Moh compared the same energy sources in addition to electromagnetic energy and identified the advantages and disadvantages of each. A recent work done by Dhananjaya and Reddy [21] considered the aforementioned energy sources in the context of the Internet-of-Things (IoT). The results from these studies show an advantage of solar energy over other energy sources in terms of power density and maturity. Therefore, this work uses solar energy as the power source for the monitoring system and combines it with thermoelectric energy harvesting from body heat to achieve self-powered operation even in the absence of light.

D. Self-powered Systems

Self-powered sensor systems have been more commonly achieved in non-wearable scenarios, especially when outdoor solar is available. However, there are examples of wearable devices being self-powered. The device presented in [22] is intended for body temperature sensing, and self-powered operation is attained with solar harvesters that have a power density of 9 μW/cm^2. The system transmits data every 134 seconds and consumes an average of 47.2 μW. Similarly, considering again the work in [12], the wearable insole uses the piezoelectric film as the sensor and as the energy source at the same time. Its average output power during normal walking is 100 μW and demonstrates an important concept in self-powered wearable devices, which is the relationship between the sensing location and the energy harvesting location. This applies to the device introduced in this work, and its implications are further discussed in the sections below. Furthermore, in [23] a more recent work implemented an autonomous wireless sensor node powered by solar energy with two functional modes. In one operation mode, the sensor node collected body temperature and heart rate data to be transmitted to an aggregator for local displaying and uploading to a web service. In the other operation mode, the node remained asleep until a fall detection event occurred and a notification to the aggregator was sent. The sensor system consumed 1.76 mW when active, and it adopted a heavily duty-cycled power management strategy to achieve lower power operation. Additionally, it is important to mention that self-powered wearable sensors have been realized through ASIC technologies as discussed in section A. That was the case of the work presented in [18] where the SoC was intended to be powered by energy harvesting from solar cells or TEGs. A similar case is the effort introduced in [24] where an SoC for EMG sensing was developed. The system consumes 24 μW when deployed and it is powered by RF energy harvesting. A more recent work presented in [25] demonstrates a system-in-package (SiP) that operates solely from energy harvesting

and has the capability to recover from power losses by integrating an ultra-low power non-volatile memory. The system is intended for different wearable applications and performing continuous ECG monitoring consumes only 1.02 µW that is delivered from solar cells or TEGs with a peak efficiency of 71.1%. All these efforts are great contributions that have pushed forward the state-of-the-art in self-powered wearable sensing. However, the robustness and technology readiness level of these systems is often far from being able to be deployed in the real world, with more naturalistic environments. Furthermore, the accessibility to this technology is very limited and it represents a high cost. The conjunction of these factors sets the aforementioned efforts as potential solutions in the long term, but leaves a gap in the near/intermediate term where other approaches such as the one presented here can promote the widespread adoption of wearable technology.

III. System Overview

The system presented in this paper is a semi-custom commercial-off-the-shelf (COTS) based self-powered sensor system designed to perform vigilant long-term cardiac and activity monitoring. The device is designed as a 3-electrode, single lead ECG that continuously samples and wirelessly streams ECG data in addition to 3-axis motion data to a smartphone. The system samples ECG data with an 8-bit resolution at 50 Hz and motion data at 12.5 Hz to achieve a low-power consumption of 683 µW while preserving vigilant sensing operation. (See Section VI for rationale behind 50 Hz @ 8 bits ECG sampling for AF detection.) Three main blocks constitute the architecture of the system: Sensing, Energy Harvesting and Power Management, and Control and Data Transmission. The Sensing block integrates a digital accelerometer and a discreet analog-front-end (AFE) that interfaces with the ECG shirt. Similarly, flexible solar cells, TEGs, a DC-DC converter for each source, a supercapacitor and a low drop-out (LDO) regulator compose the Energy Harvesting and Power Management block. Finally, the Control and Data Transmission block is comprised of a BLE-enabled system-on-chip (SoC) from Dialog Semiconductors. A block diagram of the architecture is shown in figure 1. Most of the components are integrated onto two small printed circuit boards (PCBs) with dimensions 2.79 cm by 2.28 cm to achieve a compact form factor and increase its wearability. The two PCBs are the energy harvesting board and the system main board. The energy harvesting board incorporates the DC-DC converters and the supercapacitor that acts as a storage element for the system. The system main board accommodates the accelerometer, the ECG AFE, the LDO regulator and the BLE SoC. This distributed architecture gives the system certain flexibility to interface with different harvesters and sensors according to the target application.

A. Sensing

The sensing modalities relevant to the defined use case application are ECG and motion, which provides activity context to the cardiac data. The Sensing block, which is integrated onto the main board, acquires the sensor data from the user and transfers it to the SoC where it is stored in a buffer for transmission. The accelerometer used for motion recording is the ADXL362 3-axis digital output MEMS accelerometer from Analog Devices. The device can operate in a voltage range of 1.8V to 3.3V and at the 2.3V domain set for the whole system, it consumes less than 5 µW of power at a 100 Hz output data rate. The accelerometer has a 12-bit data resolution, from which only 8 bits are used in this application for power reduction, and the measurement range is set from -2g to +2g according to the characteristics of human motion. The device incorporates a standard Serial Peripheral Interface (SPI) that allows it to communicate seamlessly with the BLE SoC.

The ECG AFE consists of six discreet LPV521 low-power, operational amplifiers (op-amps) from Texas Instruments. The initial stage integrates four op-amps in an instrumentation amplifier configuration with a set gain of 110 and a passive, low-pass filter at the input with a cutoff frequency of 1.5 KHz. The purpose of this filter is to remove high frequency noise that could be coupled to the leads of the electrodes. At the output of the instrumentation amplifier, an additional active, second-order, Sallen Key low-pass filter with a cutoff frequency of 135 Hz was implemented. Finally, a driven right leg (DRL) circuit was included to reduce common-mode interference. The measured Common Mode Rejection Ratio (CMRR) for our design corresponds to 106.8 dB. Additionally, the overall ECG

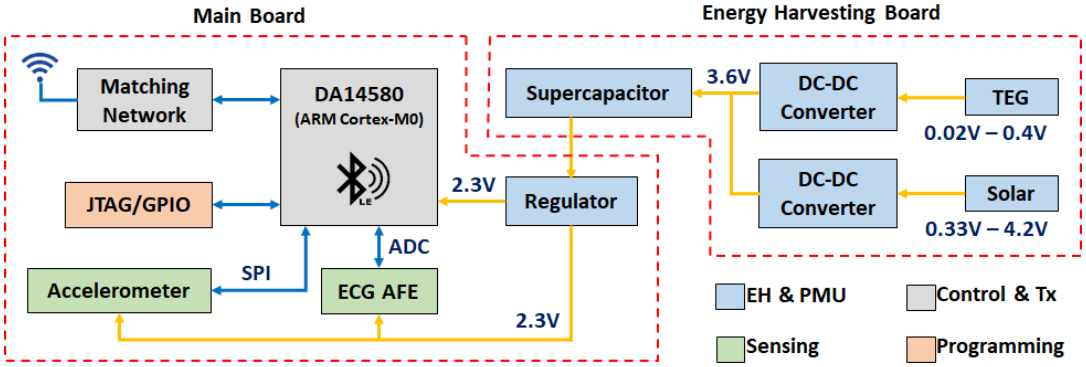

Fig. 1. Block diagram of the self-powered system with the three main modules that comprise it. The system is distributed onto two PCBs: main board and energy harvesting board.

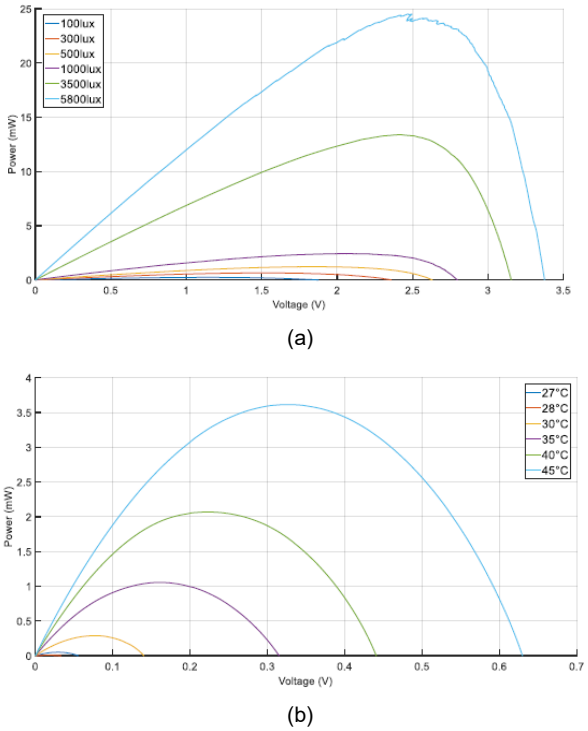

Fig. 2. Characterization of the energy harvesting arm band: (a) Output power of the solar cells for different levels of illumination; (b) Generated power from the TEGs on a hot plate at 32 °C and under several ambient temperature conditions.

AFE presents an input referred noise of 0.398 mVrms. The AFE can operate with a power supply as low as 1.6V, where a minimum power consumption of 46.6 µW is achieved. After the signal conditioning, the output of the ECG AFE interfaces with the analog to digital converter (ADC) of the BLE SoC that digitizes the signal with a resolution of 10 bits, where the 8 most significant bits are extracted for further processing. Additionally, the ECG AFE incorporates a 3.5mm audio jack to have the flexibility of interfacing with standard patch electrodes or, in this case, the custom ECG shirt.

B. Energy Harvesting and Power Management

The Energy Harvesting and Power Management block administers and supplies power to the Sensing and Control and Data Transmission blocks by extracting the available power from the solar cells and TEGs. The selected flexible solar cells are the MP3-37 and LL200-3-37 from Power Film Solar with a nominal open circuit voltage of 3.2 V and with a combined surface area of 166.44 cm^2. The DC-DC converter selected to interface with the solar cells was the BQ25505 ultra-low power boost converter from Texas Instruments given its wide input voltage range and the on-chip maximum power point tracking (MPPT) circuit. In the case of solar cells, the MPP is typically located between 70% and 80% of their open circuit voltage. The converter extracts the maximum power available by modulating the input impedance of the device to the one from the solar cells using a pre-set resistive divider. The open circuit voltage is sampled every 16 s for 256 ms to adjust the duty cycle of the converter accordingly. For the operating conditions of the selected solar cells under most scenarios, the device presents an

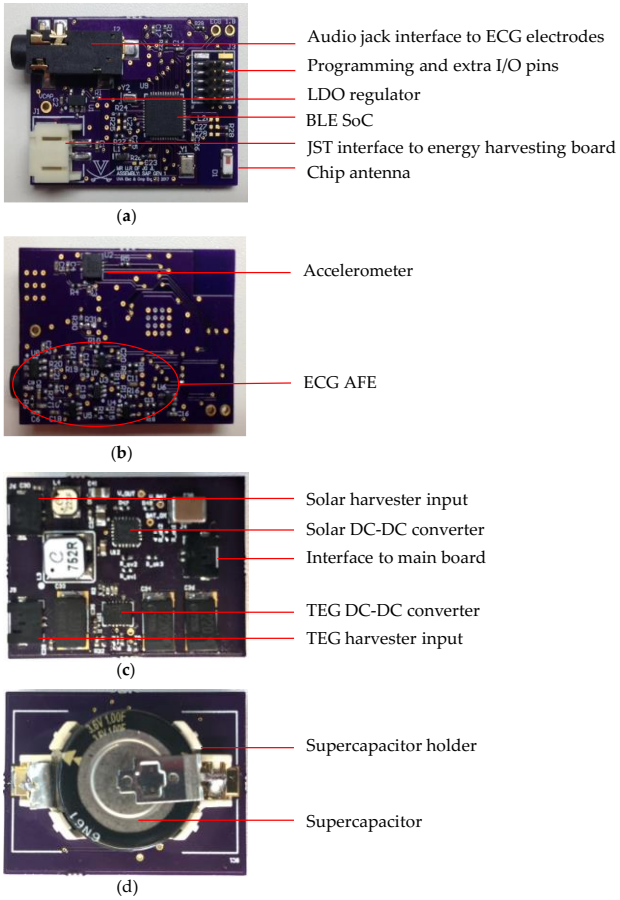

Fig. 3. The self-powered wearable sensor system: (a) Top side of the main board (2.79 cm x 2.28 cm); (b) Bottom side of the main board; (c) Top side of the energy harvesting board (2.79 cm x 2.28 cm); (d) Bottom side of the energy harvesting board.

efficiency between 80% and 90% and autonomously administers the harvested energy over two paths, one to power the system main board and another to store the excess energy onto a supercapacitor that powers the system when there is not enough energy available at the input. To complement the solar cells, the SP5424 TEGs from Marlow Industries were selected to provide power under little to no-light conditions. An array of 20 TEGs with an effective surface area of 17.43 cm^2 was created and were incorporated into an arm band as discussed in section 4. Since TEGs produce a small output voltage under wearable conditions, an ultra-low voltage boost converter was required. The LTC3108 from Linear Technology is capable of operating from 20mV inputs with a trade-off of lower efficiency (30 – 40%) given the losses at the input stages (transformer, rectifier, gate drive) necessary to operate from these lower input voltages. To achieve the ultra-low voltage operation, the device uses an external transformer to create an oscillator and amplify the signal to later rectify it. The transformer ratio determines the input voltage range at which the boost can function appropriately, in this case 20mV to 400mV for a 1:100 ratio. Similarly to the BQ25505, the LTC3108 manages the harvested energy in such way that the surplus energy is stored in a capacitor. For this application, a 1F supercapacitor was selected as the storage element, and it was connected to the storage path

(a) (b)

Fig. 4. Screenshot of the developed applications for data display: (a) Cloud interface displaying ECG and acceleration data; (b) Android application with ECG and acceleration data displayed.

of both converters. Finally, an LDO regulator – TPS78326 from Texas Instruments – generates the 2.3 V rail needed for powering the accelerometer, the AFE, and the BLE SoC. Figure 2 presents power vs. voltage curves for the solar cells and TEGs integrated into an arm band under different ambient conditions. For this assessment, the LITE platform presented in [26] was used in the evaluation of the solar cells. In the case of the TEGs, a hot plate and a fan were used to create and sustain a desired temperature difference.

C. Control and Data Transmission

The Control and Data Transmission block controls the sensor data flow and wirelessly transmits it to a smartphone. The BLE SoC used is the DA14580 from Dialog Semiconductor. This device incorporates 32 digital general purpose I/O (GPIO) pins, a SPI bus, and four 10-bit ADC channels. The SPI bus is used to communicate with the accelerometer, and one of the ADC channels is used to digitize the ECG signal. The DA14580 uses a 16 MHz 32-bit ARM Cortex-M0 for processing and a designated BLE core compliant with the BLE 4.2 standard. The BLE transceiver has a configurable output power that can be set to 0dBm or -20dBm. In this system, the second mode was selected to reduce power consumption. The SoC contains four memories: an 84 kB ROM for the BLE protocol stack and the boot code sequence for start-up, a 32 kB one-time programmable (OTP) memory to store the application code and the BLE profiles, a 42 kB system SRAM for mirroring the application code from the OTP upon wake up from sleep mode, and a series of low leakage SRAM cells for various data of the BLE protocol and to store the processor stack when the system goes into deep sleep mode. Figure 3 shows the system main board and the energy harvesting board.

After transmission, the sensed data is displayed locally using a smartphone and remotely using a web application. A custom Android application was developed to display the data on the smartphone, which also uploads it to a time-series database hosted by Amazon in the current version. The view and display of the data is performed by a platform called Grafana. In figure 4, screenshots of the Android application and the web application are presented.

IV. Textile Integration

In an effort to address the issue of user compliance by improving system wearability, several garments to integrate different harvesters were designed, and a custom ECG shirt was developed.

A. Energy Harvesting Garments

The first approach to integrate a harvester into clothing was to attach solar cells to a compression arm sleeve. The cells were placed and sewed to the arm sleeve at the forearm level given the higher exposure to light of this area. On the upper arm, a small pocket to hold the main board and energy harvesting board was similarly sewed, and the leads coming from the solar cells were run inside the sleeve to the pocket to connect to the energy harvesting board. Even though this solution was able to harvest enough energy to maintain the system running at low sampling frequencies under indoor light conditions (469 lux average, 5000K fluorescent), the energy was not enough to fully recharge the 1F supercapacitor during the day if the lighting conditions did not change considerably, preventing the system from functioning for long periods of time in dark environments (e.g. at night).

The second solution, and considering that the shoulders would have a higher exposure to light relative to the forearm, a solar shirt was designed. For this garment, smaller, rigid, amorphous solar cells were used since they perform better under low light conditions. In this case, assuming that the shirt may need to be washed, small Velcro straps were sewed to the shoulder of the shirt and similarly glued to the back of the solar cells to have the flexibility of attaching and removing the cells as needed. The results from testing the shirt showed that even though the exposure to light increased, the rigid cells were still not producing enough energy that ensured the operation of the system overnight.

Finally, using the knowledge acquired from the previous two solutions, a third garment that incorporated multiple flexible solar cells and TEGs was created. In this approach, two new low-light flexible solar cells were added to the array used in the arm sleeve to increase the energy harvested from light, and the TEGs were added to work as a backup for dark environments

using the body heat as the energy source. The multiple harvesters were integrated in an arm band meant to be worn on the upper arm. The solar cells were attached on the anterior upper arm, and the TEGs were placed on the interior. The arm band also included a small pocket to carry the sensor system, and buttonholes were designed to run the harvester and ECG cables. This solution harvests a higher amount of energy when the illumination levels are very low and enough to charge the supercapacitor in relatively short periods of time when outdoors. Although the power harvested from the TEGs is small compared to the solar cells (as was expected), this small amount is able to extend the operation of the system when no harvesting from the solar cells is possible.

B. ECG Shirt

A custom e-textile shirt acquires the ECG signal for the system. The shirt utilizes three dry electrodes integrated into a knitted compression fabric supplied from Hanesbrand Inc., NC, USA, made of 87% polyester and 13% spandex yarns with a basis weight of 150 g/m2. The electrodes were screen printed with Creative Materials (124-36) Ag/AgCl electrically conductive ink onto a thermoplastic polyurethane film (TPU) obtained from BEMIS Inc. (TL644), and heat laminated onto the knitted compression fabric. The composite like structure of the textile-based electrodes results in a durable and stretchable

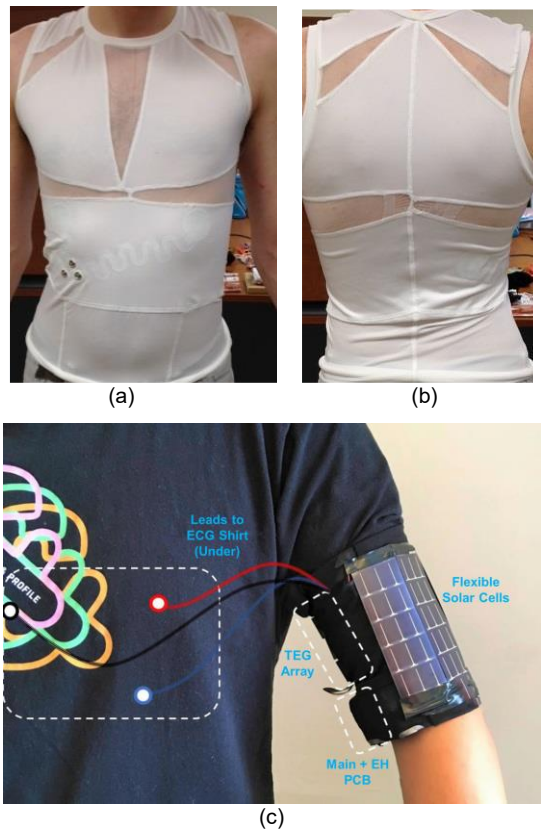

Fig. 5. Custom ECG shirt with dry electrodes on the body: (a) Front view of the ECG shirt with the snap button connectors on the left to interface with the main board; (b) Back view of the ECG shirt, the electrode for reference can be seen on the right lower back; (c) Full integration of the ECG shirt (under) with the system boards and the energy harvesting arm band.

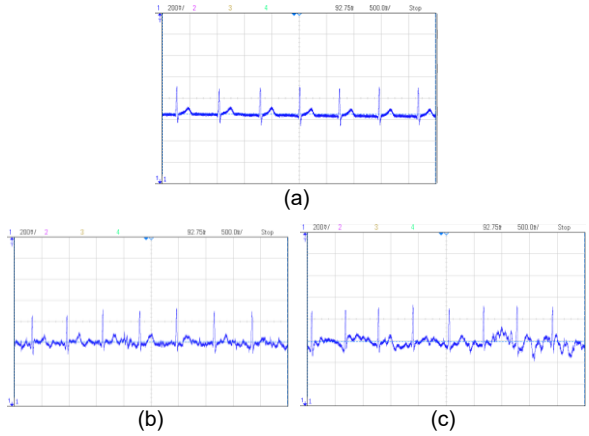

Fig. 6. ECG signal acquired with the custom ECG shirt and the implemented AFE displayed on an oscilloscope. (a) ECG signal when user is still; (b) ECG signal when user is running in place; (c) ECG signal when user is dancing.

electrode with excellent electromechanical properties [27]. In contrast with common ECG sticky electrodes, the developed dry electrodes do not produce irritation on the skin and allow for long term monitoring and data collection. Regarding the structure of the shirt, in addition to using the form-fitting knitted compression fabric, the shirt employs a custom panel design. The transparent panels incorporate another type of compression fabric whose elasticity is higher than the Hanesbrand knitted compression fabric. The chosen fabrics and custom panel design help the shirt conform to the user's body as tightly as possible and maintain good skin-electrode contact. Skin-electrode impedance is a key parameter when acquiring high-fidelity ECG signals and is directly correlated to the contact of the skin relative to the electrode [28]. Poor skin-electrode contact results in a high skin-electrode impedance and low-quality ECG signals. An evaluation of skin-electrode impedance for our shirt done from 0.1 Hz to 1000 Hz showed an impedance range of 10 KΩ to 550Ω, respectively. Figure 5 shows the ECG shirt on the body and demonstrates effective compression in the areas where the ECG electrodes are located. The three metal knobs in figure 5a are the snap connection points for the ECG cable that connects the shirt to the main board.

The shirt has good compression in most areas, but it is heavily dependent on the user's anatomical physique. Thus, it can be difficult to get the electrodes to establish good skin-electrode contact at all times. The particular shirt seen in figure 5 was sized to dimensions slightly different than the user's physique. The slight sizing variance results in wrinkling of the shirt as seen in figure 5b. Wrinkling is problematic because it can cause poor skin-electrode contact and low ECG signal quality. Physiological factors such as dry skin can also affect the ECG signal quality from the shirt. This is a problem independent of skin-electrode contact because dry skin is a poor conductor, which increases the overall skin-electrode impedance. Different solutions can be utilized to overcome these setbacks. The first, and probably least practical in day-to-day situations, is to work up a sweat. The ions in sweat turn skin into a better conductor and help the electrodes stick in place

preventing wrinkles from moving them around. The second more practical solution is to put lotion on the skin where the textile-based electrodes make contact. The lotion acts as an electrolyte, similar to those found in commercially available wet electrodes. This decreases the overall skin-electrode impedance and helps the electrodes stick in place, similar to the effect of sweating.

If proper skin-electrode contact is maintained, the resulting connection and acquired signal are quite robust. This was verified by measuring the ECG signal from the shirt when performing different movements and comparing those signals to an ECG signal acquired when performing no movement. These tests were also conducted to quantify and understand the skin-electrode contact throughout the different movements. The motions performed were running in place and dancing. Running in place was performed to test the effect of consistent movement, while dancing was performed to test the effect of erratic movement. We determined the signal-to-noise ratio (SNR) for each activity using MATLAB wavelet signal denoising method and found an SNR of 36.9 dB for no motion, 25 dB for running and 21.9 dB for dancing. The captured ECG signals for each of these tests are shown in figure 6. Both types of movement introduce more noise into the ECG signal compared to the no motion evaluation. The noise in the signal is correlated to the custom panel design of the shirt. The transparent panels seen in figure 5 have a higher elasticity than the fabric integrated with the electrodes located on the torso of the shirt. The higher elastic fabrics act as a buffer by absorbing most of the motion generated from both movements. This helps isolate the fabric integrated with electrodes from motion artifacts experienced from both types of movements. As a result, the ECG signal was never lost, nor was the noise large enough to significantly distort the waveform and prevent the measurement of key features such as the R-R interval used in this approach.

V. Power Consumption Modeling

The total power consumption of the system and its relationship with the sampling rate was modeled by the following equations:

$$P_{tot} = P_{cmpts} + P_{BLE} \quad (1)$$

$$P_{BLE} = \frac{fT_cT_{as}P_{as}+T_{at}P_{at}+(T_c-T_{at}-fT_cT_{as})P_s}{T_c} \quad (2)$$

where P_{cmpts} represents the power consumption of the accelerometer, the ECG AFE, and the LDO regulator; and P_{BLE} constitutes the power consumption of the BLE SoC. P_{BLE} is dynamic and it is defined by the duty-cycling activity between operation modes in the BLE SoC as illustrated in figure 7. Essentially, the BLE SoC wakes up from sleep mode and goes into active mode periodically to sample data from the sensors. This data is stored in a 20-byte buffer. Once the buffer is full, packets containing the data are sent in a connection event to the smartphone.

In equation 2, P_{BLE} is calculated from the sampling rate of the sensors, the length of the connection interval, and the transmission period for each packet. T_c represents the length of the connection interval. T_{as} represents the period of time when the BLE SoC is active for sampling data. T_{at} represents the transmission time. The power consumptions of the BLE SoC active and sampling, transmitting, and sleeping are represented by P_{as}, P_{at}, and P_s, respectively.

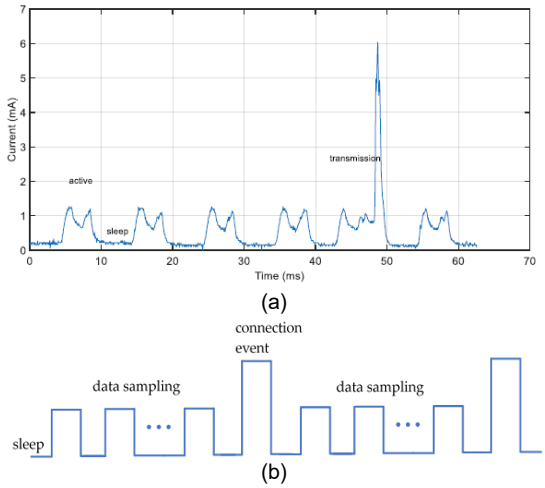

Fig. 7. System power modeling using the workload operation profile. a) Workload profile during normal operation. Three states are observed: active, sleep and transmission, b) Power profile representation based on the workload profile for normal operation [10]. During the active mode, the data is sampled and when a connection event occurs, the data is transmitted to the phone.

P_{BLE} is also calculated from the sampling frequency of the sensors. A plot of the sampling frequency vs. system power is shown in figure 8. As seen in the plot, the system power increases linearly with frequency. Since the sampling rate is the most easily controllable variable in P_{BLE}, modeling system power in this way is useful for determining the optimum sampling rate at which to run the system given a specified power budget. For example, for the system to consume less than 450 µW, the sampling rate has to be 25 Hz or below. However, it is also important for the sampling rate to be high enough to capture all the important features of the ECG signal based on the application requirements. The decision to use 50 Hz as the sampling frequency to maintain cardiac vigilant monitoring is discussed in the following sections. Table 1 summarizes measured power consumption of the self-powered system and individual modules for comparison with the projected values from figure 8. The discrepancy between the estimated power

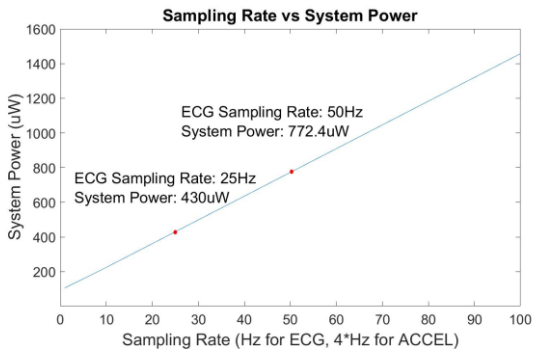

Fig. 8. Projected system power consumption using the power model for different sampling rates modified from [10].

TABLE I
SYSTEM POWER BREAKDOWN

Component	Power (μW)
ECG AFE	67
Accelerometer	4.55
LDO Regulator	9
BLE SoC Sleep Mode	9
BLE SoC Active Mode	1598
Total System Power (ECG (50 Hz) + motion (12.5 Hz) monitoring)	**683**

consumption from the model and the corresponding power measurements are attributed to the fact that the numbers entered in the model correspond to the maximum power values derived from the datasheet for each component in the system and therefore representing the worst-case scenario.

VI. VIGILANT ATRIAL FIBRILLATION MONITORING

AF is a condition characterized for abnormal heart rhythm commonly associated with heart diseases such as cardiac failure. The early detection and diagnosis of AF could help to prevent heart failure and stroke, but vigilant monitoring is necessary to capture transient periods of AF.

In a patient with AF, the irregularly rapid action potentials produced in the atrium manifest in the ECG as low amplitude potentials that alter the ECG baseline, often masking the P-wave. As these irregular atrial action potentials travel through the heart's electrical system, they reach the AV node and generate ventricular activity that is presented in the ECG as a QRS complex. Given the refractory period of the AV node, not all of the irregular atrial action potentials can trigger ventricular activity. As a result, the ECG of an AF patient is characterized by the absence of P-waves and irregular QRS complex. Given these characteristics of the condition, the analysis of R-R intervals and atrial activity waveforms are two of the main methods for AF detection. In a comparative study for AF detection reported in [29], the algorithm performance for both approaches was evaluated, and it was concluded that the R-R interval-based approach provided better results. Therefore, an R-R interval approach was adopted in this work.

The R-R interval variations are used in different ways for AF detection. In [30], a normalized R-R interval variation threshold is set to classify AF events. In other works, both R-R interval and its change are used for detection of AF [31]. In [32], the Kolmogorov-Smirnov test is used to detect AF episodes. In this paper, we used the method in [30] for its simplicity and high performance. For R-R interval calculation, we used the curve length transform in [33] and additional methods such as a wavelet transform [34]. The curve length transform algorithm can deal with baseline changes using a dynamic threshold.

The original ECG data employed in the exploration was retrieved from the MIT-BIH AF database [35], number 05121. The data was collected using ambulatory Holter monitors with a sampling frequency of 250 Hz. The total length of the recordings corresponds to 10.23 hours, which contains 26 AF events and junctional premature episodes that comprise 6.51

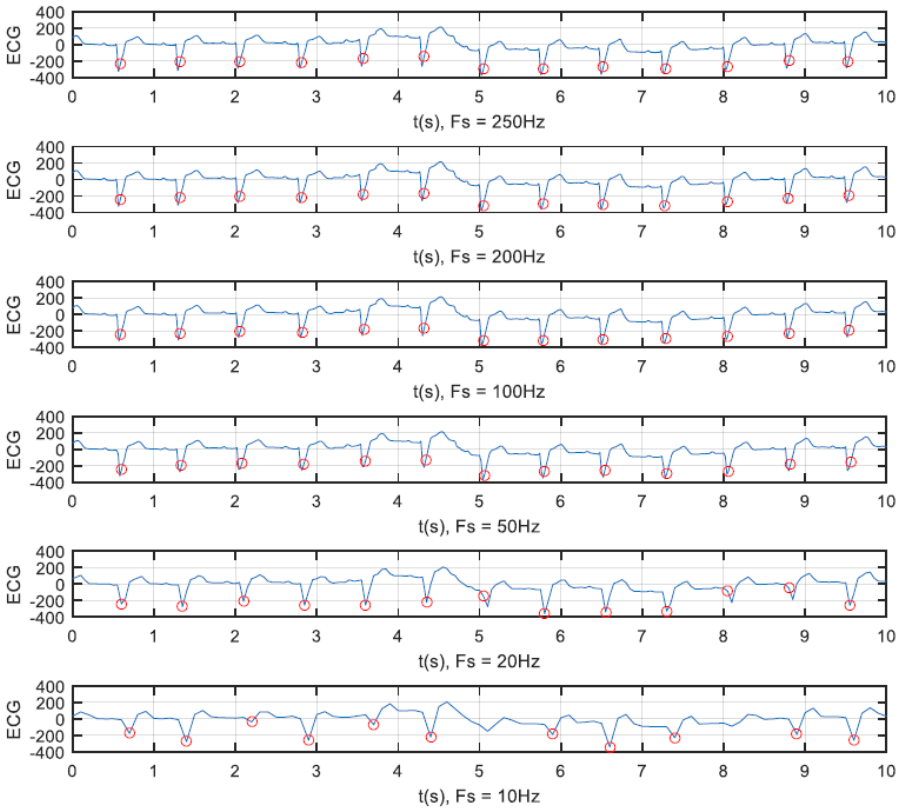

Fig. 9. ECG waveforms and detected R peaks in red circles with different sampling rates. With the decrease in sampling rate, the ECG signal becomes distorted, but the R peak detection works well until a minimum sampling rate of 20Hz. Modified from [11].

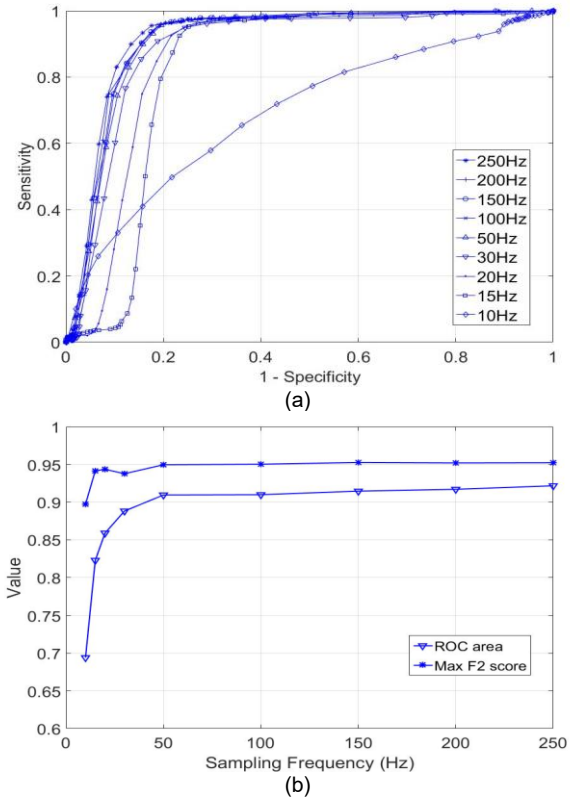

Fig. 10. From [11]. a) The receiver operating characteristic (ROC) curve of AF detection under 9 sampling rates. The curve is moving inward as the sampling rate decreases, b) The ROC area and maximum F2 score across different sampling rates of ECG data.

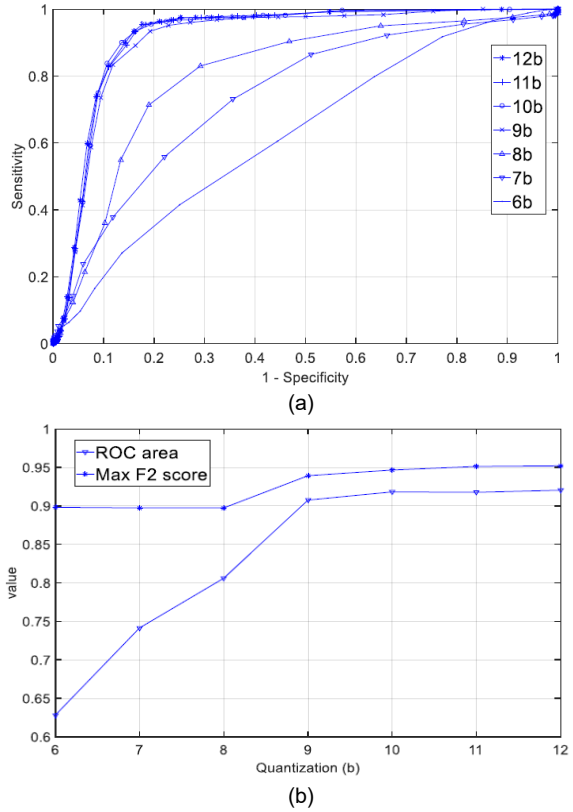

Fig. 11. a) The receiver operating characteristic (ROC) curve of AF detection corresponding to seven bit depths. The curve is moving inward as the bit depth decreases, b) The ROC area and maximum F2 score across different bit depths of ECG data.

hours out of the total length. The WFDB MATLAB Toolbox [36, 37] was used for reading the ECG signal and annotations. In the experiment, the raw ECG signal is downsampled to simulate low sampling rate scenarios. Then the AF detection with R-R interval calculation algorithm is executed using the downsampled ECG signals. The R-R interval calculation algorithm was reimplemented from [33] to tune the parameters for dealing with low sampling frequency scenarios. Figure 9 shows a 10 second window of ECG data at the original sampling frequency and five down-sampled versions.

To quantitatively evaluate the performance of the AF detection algorithm with respect to the sampling frequency, the receiver operating characteristic (ROC) curve was created considering 9 different sampling rates from 250 Hz to 10 Hz. The resultant family of curves is shown in figure 10a. In general, it is possible to see the curve moving inwards as the sampling rate decreases. Furthermore, to expand the evaluation, the ROC area and the maximum F2 scores were calculated. The results are illustrated in 10b. The ROC area corresponds to the area under the ROC curve and the F2 score considers both

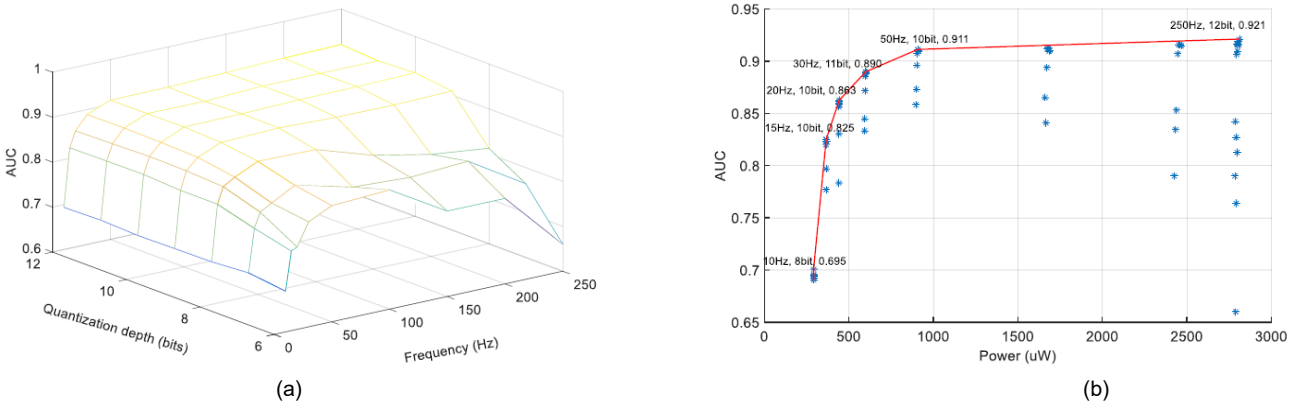

Fig. 12. a) The ROC area versus bit depth and sampling rate, b) Design space considering sampling rate and bit depth. The red line represents the optimal design specification for a given power consumption level.

TABLE II
COMPARISON OF LOW POWER, WEARABLE, ECG SYSTEMS

	[33]	[34]	[35]	[36]	[37][1]	[38][1]	[39]	This Work
Number of electrodes	2	3	3	3	4	3	2	3
ADC (bits)	8	n/a	12	16	24	12	16.5 (14 ENOB)	8
fs_{ECG} (Hz)	300	n/a	200	500	500	750	320	50
Voltage (V)	n/a	3	3	1.8	3	3.3	3	3
Power (µW)	n/a	12500	137	6500	90000	13400	12000	683
Communication Protocol	BT	BT	BLE	BLE	BT	BLE	ZigBee Pro	BLE
Multimodal Sensing	Yes	No	Yes	No	Yes	Yes	No	Yes
Web Access	Yes	No	No	No	No	Yes	Yes	Yes
Vigilant Operation	Yes[2]	Yes[2]	No	n/a	Yes[2]	Yes[2]	Yes[2]	Yes
Data Storage	Local / Remote	Local	Remote	Remote	Local / Remote	Local / Remote	Remote	Remote
Power Source	Battery (48 hrs)	Battery (30 hrs)	TEG (Self-powered)	n/a	Battery (5 hrs)	Battery (96 hrs)	Battery (160 hrs)	Photovoltaic + TEG (Self-powered)
Dimensions (mm)	90 x 40 x 16	58 x 50 x 10	60 x 32 x n/a	24 x 14 x n/a	30 x 25 x 10	13 x 11 x 5	65 x 34 x n/a	28 x 23 x 12

[1] System operating in streaming mode. [2] Vigilant operation only during battery lifetime.

classification recall/sensitivity and precision, and weights recall higher to reduce the false negative rate (failed to detect AF). For each sampling rate, the maximum F2 score was calculated over the set threshold.

For both curves, the value generally increases with higher sampling rate. For the ROC area, the performance increases fast when the sampling rate is low, and it sees diminishing returns when the sampling rate is higher. In addition, from the curves it is possible to see that the performance almost reaches saturation after 50 Hz, which makes it the minimum power operating mode for vigilant AF monitoring.

A similar analysis looking at the effects of bit depth on the sampled ECG signal was conducted. For this matter, the ROC, ROC area and F2 score were computed over different quantization depths going from the original 12 bits to 6 bits as illustrated in figure 11.

To complete the analysis, the ROC area results for sampling rate and bit depth were combined in to establish the relation of these two parameters and the overall average system power consumption. The 3D plot of the ROC area is presented in figure 12a. It is possible to see that the ROC area, representing the performance of the system, is directly proportional to the sampling rate and bit depth. However, some irregularities when the bit depth is below 8 bits are identified. Under these conditions, the above relation does not hold. The main reason for this behavior is that the initial classification result is smoothed using a majority vote. Under the low bit depth scenarios, the R-R interval computation performs poorly, but the smoothing may increase the performance regardless of the sampling rate. Nevertheless, the signal quality below 8 bits is too low and therefore is not considered for real-world monitoring. Furthermore, employing the power consumption model defined by equations (1) and (2) in Section V, the design space considering the two discussed parameters and their possible combinations is denoted by the blue markers in figure 12b. The red line is part of the convex hull of all the points and it represents the optimal design specifications for a given power budget.

VII. COMPARISON WITH STATE-OF-THE-ART

To highlight the contributions of this work, the proposed system was compared to similar COTS based, state-of-the-art cardiac monitoring devices [39-44] and commercially available solutions [38]. To present a fair comparison, the selected systems had to feature three main characteristics: low power operation, small form factor for wearability, and wireless connectivity. Based on these criteria a set of 12 categories were defined, and the results are summarized in Table 2. From this information it is possible to notice how most of the devices operate at 3V, have a relatively small form factor and present a 3-electrode configuration with a DRL circuit for a higher CMRR and reduction in the ECG baseline wandering. The bigger differences among the solutions are observed in the bit depth, sampling frequency, power consumption and operation mode.

The strengths of the proposed system are the low power consumption (only 683 µW), its continuous, vigilant operation, and the end-to-end system integration for remote monitoring. While all of the compared solutions can operate continuously, none of them features a true vigilant characteristic for long-term monitoring given the limited battery lifetime. A special case is the Ultra-Low Power Sensor Evaluation Kit (ULPSEK) presented in [40], where energy harvesting is used as the power source. The system achieves the lowest power consumption and self-powered operation, but heavy duty-cycling is required. Its implemented power management scheme wakes up the device to sample the sensor data for 31 seconds and then puts it to sleep for 12 minutes to reduce the average power consumption to 137 µW over the 12.5-minute window. Therefore, ULPSEK is a

self-powered system with near-continuous operation but does not provide vigilant monitoring for cardiac event detection. Even though the work presented in this paper has lower numbers in terms of bit depth and sampling frequency, these parameters were set based on the application-driven approach to optimize power consumption while ensuring data quality.

VIII. Deployment Results And Considerations

The sensor system was deployed on a healthy male individual for two consecutive days to evaluate its performance.

Before the deployment, the storage element – a supercapacitor – was sized to ensure operation during prolonged periods of time when no harvesting was possible. Through experimental methods, three different custom supercapacitors were evaluated: 1F, 1.9F and 3.5F [45]. The experiment consisted of letting the sensor system run normally with only the fully pre-charged supercapacitor as the power source. For each of the capacitances, the recorded run times were 3.3 hours, 6.02 hours and 12.65 hours, respectively. The supercapacitors used had a form factor similar to a CR2032 coin cell battery, thus the wearability was not compromised.

With all the system elements in place, the individual was asked to wear the system while doing his regular activities. To determine the impact of changes in illumination, the voltage of the storage element was randomly monitored, and the only time the voltage dropped was at night when no light was available – a positive energy balance was maintained at all other times. For the two mornings of the deployment, the individual reported to measure approximately 2.1V in the storage element after waking up, with the system still powered on and streaming data to the phone, supported in part by the TEG harvesting. During the day, it took about 6 hours for the storage element to be fully charged in an indoor environment of ~500 lux. Based on our previous profiling work [46, 47], the average illumination level at the office is 537 lux, which indicates that the conditions for the storage element to be recharged can be normally met.

In the case of individuals with less mobility and those who spend most of the time in low illumination environments, the vigilant operation of the system may be compromised. For instance, in a scenario where the system is operating at a low voltage (e.g., morning after overnight operation) and the average illumination exposure during the day is 250 lux, the system will be able to operate while the light source is present, but it may not stay on for a long time with no solar harvesting (e.g., the following night).

Typical illumination levels outdoor are higher than 100,000 lux on a clear day and 20,000 lux on a cloudy day. In the case of indoor environments, the illumination levels are in the range of 100-1000 lux. If the average illumination level over 12 hours is higher than 300 lux, the supercapacitor will be fully recharged. A study presented in [48] surveying national human activity patterns reported that the average American spends 87% of their time indoors, 6% in enclosed vehicles and 7% outdoors. This last number represents 1 hour and 40 minutes under illumination conditions higher than 1000 lux given that most of the activities corresponding to this percentage occurred between 7 AM and 6 PM according to the study. With these numbers, the proposed work represents a feasible solution for the majority of the population in the U.S.

IX. Conclusions And Future Work

This paper presents a set of contributions developed to realize a platform for self-powered vigilant cardiac and activity monitoring, thereby addressing some of the critical barriers to widespread adoption of long-term remote patient monitoring. The sensor system represents a significant advancement in self-powered multi-modal harvesting and sensing by collecting and transmitting ECG and motion data in real time to a smartphone for local access and to the web for remote analysis and alerts. Vigilant AF monitoring was investigated as a typical case study, and the implications of reduced ECG sampling rate and bit depth quantization in AF detection performance were analyzed. From this analysis, it was determined that ECG signals sampled under 20 Hz are not sufficiently accurate for peak detection of the QRS complex. In addition, while sampling rates above 20 Hz and below 50 Hz can perform well in peak detection, their timing is not precise enough for accurate R-R interval extraction, which is critical for AF detection. It was therefore determined that 50 Hz is the minimum sampling rate for vigilant AF monitoring. A similar conclusion was drawn for the analysis of ECG signal quantization, and it was determined that resolutions lower than 8 bits are not feasible to guarantee the quality of the signal for AF detection. The presented sensor system operating with a sampling frequency of 50 Hz and 8 bits consumes 683 μW on average. This harvested power can be delivered by wearable solar cells in most indoor illumination levels and complemented with TEGs for operation in low-light conditions. With the integration of the ECG shirt, the wearability of the system is highly improved and the realization of long-term monitoring is enabled by using dry electrodes which do not cause irritation on the skin as their counterpart do. Furthermore, given its anatomical design and the use of compression fabrics, motion artifacts commonly seen in other ECG systems are minimized. Future work includes the exploration of different harvesters and sensors, the integration of harvesters onto textiles, and a clinical trial using the developed sensor system and the custom ECG shirt.

References

[1] S. B. Dunbar, O. A. Khavjou, T. Bakas, G. Hunt, R. A. Kirch, A. R. Leib, R. S. Morrison, D. C. Poehler, V. L. Roger, and L. P. Whitsel, "Projected Costs of Informal Caregiving for Cardiovascular Disease: 2015 to 2035: A Policy Statement From the American Heart Association," Circulation, vol. 137, no. 19, Aug. 2018.

[2] G. Giamouzis, A. Kalogeropoulos, and V. Goergiopoulou, "Hospitalization Epidemic in Patients with Heart Failure: Risk Factors, Risk Prediction, Knowledge Gaps, and Future Directions," *J. Card. Fail.*, vol. 17, no. 1, pp. 54-75, 2011.

[3] C. Davis, M. Bender, T. Smith, and J. Broad, "Feasibility and Acute Care Utilization Outcomes of a Post-Acute Transitional Telemonitoring Program for Underserved Chronic Disease Patients," *Telemed J E Heal.*, vol. 21, no. 9, pp. 705–13, 2015.

[4] B. P. Lo, H. Ip, and G.-Z. Yang, "Transforming Health Care: Body Sensor Networks, Wearables, and the Internet of Things," *IEEE Pulse*, vol. 7, no. 1, pp. 4–8, 2016.

[5] J. H. M. Bergmann and A. H. McGregor, "Body-worn sensor design: What do patients and clinicians want?" *Ann. Biomed. Eng.*, vol. 39, no. 9, pp. 2299–2312, 2011.

[6] J. Dieffenderfer *et al.*, "Low Power Wearable Systems for Continuous Monitoring of Environment and Health for Chronic Respiratory

Disease," *IEEE J. Biomed. Heal. Informatics*, vol. 20, no. 5, pp. 1–1, 2016.

[7] V. Misra, A. Bozkurt, B. Calhoun, T. Jackson, J. Jur, J. Lach, B. Lee, J. Muth, O. Oralkan, M. Ozturk, S. Trolier-McKinstry, D. Vashaee, D. Wentzloff, and Y. Zhu, "Flexible Technologies for Self-Powered Wearable Health and Environmental Sensing," *Proceedings of the IEEE*, vol. 103, no. 4, pp. 665-681, April 2015.

[8] W. Dargie, "Dynamic power management in wireless sensor networks: State-of-the-art," *IEEE Sens. J.*, vol. 12, no. 5, pp. 1518–1528, 2012.

[9] B. Srbinovski, M. Magno, B. O'Flynn, V. Pakrashi, and E. Popovici, "Energy aware adaptive sampling algorithm for energy harvesting wireless sensor networks," *IEEE Sensors Appl. Symp.*, no. 12, pp. 1–6, 2015.

[10] L. Lopez Ruiz, M. Ridder, D. Fan, J. Gong, J. Lach, and J. Strohmaier, "SCAVM: A self-powered cardiac and activity vigilant monitoring system," *2017 IEEE Biomedical Circuits and Systems Conference (BioCAS)*, 2017

[11] D. Fan, L. Lopez Ruiz, and J. Lach, "Application-driven dynamic power management for self-powered vigilant monitoring," *2018 IEEE 15th International Conference on Wearable and Implantable Body Sensor Networks (BSN)*, 2018.

[12] Y. Han *et al.*, "A self-powered insole for human motion recognition," *Sensors (Switzerland)*, vol. 16, no. 9, pp. 1–12, 2016.

[13] L. González-Villanueva, S. Cagnoni, and L. Ascari, "Design of a wearable sensing system for human motion monitoring in physical rehabilitation," *Sensors (Switzerland)*, vol. 13, no. 6, pp. 7735–7755, 2013.

[14] A.-K. Witte and R. Zarnekow, "Transforming Personal Healthcare through Technology - A Systematic Literature Review of Wearable Sensors for Medical Application," *Proc. 52nd Hawaii International Conference on System Sciences*, 2019.

[15] J. M. Pevnick, K. Birkeland, R. Zimmer, Y. Elad, and I. Kedan, "Wearable technology for cardiology: An update and framework for the future," *Trends in Cardiovascular Medicine*, vol. 28, no. 2, pp. 144–150, 2018.

[16] X. Zhang, Z. Zhang, Y. Li, C. Liu, Y. X. Guo, and Y. Lian, "A 2.89 μW Dry-Electrode Enabled Clockless Wireless ECG SoC for Wearable Applications," IEEE Journal of Solid-State Circuits, pp. 1–12, 2016.

[17] H. Bhamra, J. Lynch, M. Ward, and P. Irazoqui, "A Noise-Power-Area Optimized Biosensing Front End for Wireless Body Sensor Nodes and Medical Implantable Devices," IEEE Transactions on Very Large Scale Integration (VLSI) Systems, vol. 25, no. 10, pp. 2917–2928, 2017.

[18] A. Klinefelter, N. E. Roberts, Y. Shakhsheer, P. Gonzalez, A. Shrivastava, A. Roy, K. Craig, M. Faisal, J. Boley, S. Oh, Y. Zhang, D. Akella, D. D. Wentzloff, and B. H. Calhoun, "21.3 A 6.45uW self-powered IoT SoC with integrated energy-harvesting power management and ULP asymmetric radios," 2015 IEEE International Solid-State Circuits Conference - (ISSCC) Digest of Technical Papers, 2015.

[19] K. Z. Panatik *et al.*, "Energy Harvesting in wireless sensor networks: A survey," *IEEE Int. Sym. Tel. Tech.*, 2016.

[20] K. Singh and S. Moh, "A Comparative Survey of Energy Harvesting Techniques for Wireless Sensor Networks," *Advanced Science and Technology Letters*, vol. 142, pp. 28-33, 2016

[21] M. Dhananjaya and M. Reddy, "A Survey of Energy Harvesting Sources for IoT Device," *Int. J. Advanced Engineering, Management and Science*, vol. 3, no. 1, pp. 33-36, 2017.

[22] A. Pokhara and B. Mishra, "Design Methodology for an Energy Neutral Health Monitoring Wireless Sensor Node," *ISED Symposium,* 2016.

[23] T. Wu, J. Redoute and M. R. Yuce, "An Autonomous Wireless Body Area Network Implementation Towards IoT Connected Healthcare Applications," *IEEE Access*, vol. 5, pp. 11413–11422, 2017.

[24] H. Bhamra, Y.-J. Kim, J. Joseph, J. Lynch, O. Z. Gall, H. Mei, C. Meng, J.-W. Tsai, and P. Irazoqui, "A 24uW, Batteryless, Crystal-free, Multinode Synchronized SoC 'Bionode' for Wireless Prosthesis Control," IEEE Journal of Solid-State Circuits, vol. 50, no. 11, pp. 2714–2727, 2015.

[25] C. J. Lukas, F. B. Yahya, J. Breiholz, A. Roy, X. Chen, H. N. Patel, N. Liu, A. Kosari, S. Li, D. A. Kamakshi, O. Ayorinde, D. D. Wentzloff, and B. H. Calhoun, "A 1.02 μW Battery-Less, Continuous Sensing and Post-Processing SiP for Wearable Applications," IEEE Transactions on Biomedical Circuits and Systems, vol. 13, no. 2, pp. 271–281, 2019.

[26] H. L. Bishop, P. Wang, D. Fan, J. Lach, and B. H. Calhoun, "Lighting IoT Test Environment (LITE) Platform: Evaluating Light-Powered, Energy Harvesting Embedded Systems," *2018 Global Internet of Things Summit (GIoTS)*, 2018.

[27] M. A. Yokus, R. Foote, and J. S. Jur, "Printed Stretchable Interconnects for Smart Garments: Design, Fabrication, and Characterization," *IEEE Sensors Journal*, vol. 16, no. 22, pp. 7967–7976, 2016.

[28] M. A. Yokus and J. S. Jur, "Fabric-Based Wearable Dry Electrodes for Body Surface Biopotential Recording," *IEEE Transactions on Biomedical Engineering*, vol. 63, no. 2, pp. 423–430, 2016.

[29] N. Larburu, T. Lopetegi, and I. Romero, "Comparative Study of Algorithms for Atrial Fibrillation Detection," *Computing in Cardiology,* pp. 265–268, 2011.

[30] B. Logan and J. Healey, "Robust Detection of Atrial Fibrillation for a Long Term Telemonitoring System," *Computers in Cardiology,* pp. 619–622, 2005.

[31] J. Lian, L. Wang, and D. Muessig, "A Simple Method to Detect Atrial Fibrillation Using RR Intervals," *AJC*, vol. 107, no. 10, pp. 1494–1497, 2011.

[32] K. Tateno and L. Glass, "Automatic detection of atrial fibrillation using the coefficient of variation and density histograms of RR and ΔRR intervals," *Med. Biol. Eng. Comput.*, 2001

[33] W. Zong, G. B. Moody, and D. Jiang, "A robust open-source algorithm to detect onset and duration of QRS complexes," *Computing in Cardiology*. 2003.

[34] I. Processing *et al.*, "Continuous wavelet transform modulus maxima analysis of the electrocardiogram: beat characterisation and beat-to-beat measurement," *J. Wavelets, Multiresolution and Information Processing,* vol. 3, no. 1, pp. 19–42, 2005.

[35] G. B. Moody and R. G. Mark, "A New Method For Detecting Atrial Fibrillation Using RR Intervals," *Proceedings of Computers in Cardiology*, 1983.

[36] A. L. Goldberger *et al.*, "PhysioBank, PhysioToolkit, and PhysioNet : Components of a New Research Resource for Complex Physiologic Signals," *Circulation*, 2000.

[37] I. Silva and G. B. Moody, "An Open-source Toolbox for Analyzing and Processing PhysioNet Databases in MATLAB and Octave," *J. Open Res. Softw.*, 2014.

[38] Alive Technologies, "Alive Bluetooth Heart & Activity Monitor." [Online]. Available: http://www.alivetec.com/alive-bluetooth-heart-activity-monitor/. [Accessed: 27-Fen-2019].

[39] F. Miao, Y. Cheng, Y. He, Q. He, and Y. Li, "A wearable context-aware ECG monitoring system integrated with built-in kinematic sensors of the smartphone," *Sensors (Switzerland)*, vol. 15, no. 5, pp. 11465–11484, 2015.

[40] A. Tobola et al., "Self-powered Multiparameter Health Sensor," *IEEE J. Biomed. Heal. Informatics*, vol. 22, no. 1, pp. 15-22, 2018.

[41] J. Zhang, S. Chan, H. Li, H. Wu, J. Wu and L. Wang, "A Flexible and Miniaturized Wireless ECG Recording System with Metal-Skin Contacts Input for Wearable Personalized Healthcare," *IEEE Int. Conf. Digital Signal Processing*, 2016.

[42] M. Caldara, D. Comotti, L. Gaioni, A. Pedrana, M. Pezzoli, V. Re and G. Traversi, "Wearable Sensor System for Multi-lead ECG Measurement," *IEEE BSN*, 2017.

[43] S. P. Preejith, R. Dhinesh, J. Jospeh and M. Sivaprakasam, "Wearable ECG Platform for Continuous Cardiac Monitoring," *IEEE EMBC*, 2016.

[44] E. Spano, S. Di Pascoli and G. Iannaccone, "Low-power Wearable ECG Monitoring System for Multiple-Patient Remote Monitoring," *IEEE Sens. J.*, vol. 16, no. 13, pp. 5452-5462, 2016.

[45] A. R. Aref, C. Chou, R. Rajagopalan and C. Randall, "Bimodal Porus Carbon Electrodes Derived From Polyfurfuryl Alcohol/Phloroglucinol for Ionic Liquid Based Electrical Double Layer Capacitors," *J. Materials Research*, pp. 1-10, 2017.

[46] D. Fan, L. Lopez Ruiz, J. Gong, and J. Lach, "Profiling, modeling, and predicting energy harvesting for self-powered body sensor platforms," *IEEE BSN*, pp. 402–407, 2016.

[47] D. Fan, L. Lopez Ruiz, J. Gong, and J. Lach, "EHDC: An Energy Harvesting Modeling and Profiling Platform for Body Sensor Networks," *IEEE J. Biomed. Heal. Informatics*, vol. 22, no. 1, pp. 33-39, 2018.

[48] N. E. Klepeis et al., "The National Human Activity Pattern Survey (NHAPS): a resource for assessing exposure to environmental pollutants," *J. Exposure Analysis and Environmental Epidemiology*, vol. 11, pp. 231-252, 2001.